International Journal of Thermal Sciences 49 (2010) 1115–1127

Contents lists available at ScienceDirect

International Journal of Thermal Sciences

journal homepage: www.elsevier.com/locate/ijts

Transient two-phase flow and heat transfer with localized heating in porous media

H.Y. Li [a], K.C. Leong [a,*], L.W. Jin [a], J.C. Chai [b]

[a] School of Mechanical and Aerospace Engineering, Nanyang Technological University, 50 Nanyang Avenue, Singapore 639798, Republic of Singapore
[b] Mechanical Engineering Department, The Petroleum Institute, Abu Dhabi, United Arab Emirates

ARTICLE INFO

Article history:
Received 8 October 2009
Received in revised form
22 December 2009
Accepted 25 January 2010
Available online 1 March 2010

Keywords:
Transient
Two-phase mixture model
Discontinuous diffusion coefficient
Porous media

ABSTRACT

The transient behavior of two-phase flow and heat transfer in a channel filled with porous media was numerically studied in this paper. Based on the two-phase mixture model, numerical solutions were obtained using the Finite-Volume Method (FVM). Two methods to treat the discontinuous diffusion coefficient in the energy equation, *i.e.* the harmonic mean method and the "modified" Kirchhoff method were compared. It was found that the "modified" Kirchhoff method was better in dealing with the rapid change in the diffusion coefficient. Three different cases, with discrete heat flux applied at (1) the upper wall, (2) lower wall and (3) both the upper and lower walls were studied. The velocity and temperature fields for these cases were discussed. The results show that the liquid and vapor flow fields, as well as the temperature and liquid saturation fields have distinctly different features with the change in heating location. An analysis of the vapor volume fraction indicates that the largest amount of vapor with the highest vapor generation rate was for the case in which the heat flux is applied from the lower wall.

1. Introduction

Two-phase flow and heat transfer in porous media is widely encountered in the engineering industry [1–3]. By using phase change in a cooling system, the heat removal capacity can be greatly increased due to the large latent heat. It is demonstrated that the use of porous media as heat sinks is an effective way to remove heat [4–7]. Thus, a system which exploits the potential of phase change in a porous media is undoubtedly a promising solution to dissipate high heat fluxes from the heat sources. Extensive studies have been carried out to enhance the knowledge of two-phase convection heat transfer in porous media [8–13]. Although steady-state investigations can provide understanding of the physics behind two-phase flow problems, the transient simulation approach would be more useful since it can reveal the evolution of the boiling process and the interactions between the liquid and vapor phases.

It is commonly accepted that the phase structure in a fluid-saturated porous medium heated from below and cooled from above, is layered after the onset of boiling, with a superheated vapor zone overlying a two-phase zone and a sub-cooled liquid zone. In the two-phase zone, both the liquid and vapor phases coexist. The visualization experiments of Sondergeld and Turcotte [8] revealed that within the liquid zone, heat transfer can occur by both conduction and convection, whereas, in the two-phase zone, heat transfer occurs mainly due to the counter-percolation between the liquid and vapor. Bau and Torrance [9–11] performed a series of experiments to investigate natural convection with phase change in low-permeability porous media. Their results showed that the two-phase zone is essentially isothermal at the saturation temperature. The vertical counter-current flow of the liquid and vapor dominates the heat transfer in the two-phase zone. Ramesh and Torrance [14] performed an analytical study of the stability of boiling in porous media. Their results revealed that for liquid-dominated systems, the buoyancy force was the main factor which causes system instability. However, in vapor-dominated systems, gravitational instability may occur.

The aforementioned works are experimental studies of natural convection boiling heat transfer in porous media. Numerical simulation of two-phase flow and heat transfer in porous media is extremely complex due to the strongly nonlinear and coupled nature of the governing equations. The involved discontinuity in the thermal properties at the phase change boundary also requires careful consideration. Traditionally, the complex problems of multiphase flow and transport in porous media were solved by the separated flow model (SFM) [15,16]. In this model, the various phases are regarded as distinct fluids with individual thermodynamic and transport properties. The mathematical governing equations are separated for each phase. The separated phases are coupled together by appropriate interface conditions. Although SFM is rather straightforward, a large number of differential equations

* Corresponding author. Tel.: +65 6790 5596; fax: +65 6792 4062.
E-mail address: mkcleong@ntu.edu.sg (K.C. Leong).

1290-0729/$ – see front matter © 2010 Elsevier Masson SAS. All rights reserved.
doi:10.1016/j.ijthermalsci.2010.01.024

Nomenclature

C_p	specific heat of fluid (J/kg K)
D_s	capillary diffusion coefficient (m^2/s)
$f(s)$	hindrance function
$\boldsymbol{g}$	gravity vector (m/s^2)
h	enthalpy (J/m^3)
h_{fg}	latent heat of phase change (J/kg)
H	height of the simulation domain (m)
$\boldsymbol{j}$	diffusive mass flux (kg/m^2 s)
$J(s)$	capillary pressure function
k	relative permeability
k_{eff}	effective thermal conductivity
K	permeability of the porous medium (m^2)
L	length of the simulation domain (m)
p	pressure (Pa)
q''	heat flux (W/m^2)
s	liquid saturation
S	energy source term (W/m^3)
t	time (s)
T	temperature (°C)
$\boldsymbol{u}$	velocity vector (m/s)

Greek symbols

β	thermal expansion coefficient ($1/K^{-1}$)
γ	Advection correction coefficient
$\Delta\rho$	$\rho_l - \rho_v$ (kg/m^3)
ρ	density (kg/m^3)
ε	porosity
λ	relative mobility
μ	dynamic viscosity (kg/m s)
υ	kinetic viscosity (m^2/s)
σ	surface tension (N/m)
Ω	effective heat capacitance ratio
Γ	diffusion coefficient
Γ_h	diffusion coefficient in enthalpy equation

Subscripts

l	liquid
o	initial state
s	solid
sat	saturation
v	vapor

have to be solved. An alternative approach, the two-phase mixture model, was developed by Wang and Beckermann [12]. In this model, the two-phase system is treated as constituents of the binary mixture. The governing equations in this model identically reduce to single-phase transport equations. The bulk behavior of the mixture is captured by this model. However, the formulations do not lose the intrinsic characteristics of the individual phases. Compared with the SFM model, the two-phase mixture model is easier to implement. Hence, it is popularly used in the study of two-phase flow in porous media. Wang et al. [17] adopted this model to numerically study boiling and natural convection in capillary porous media. Four different flow patterns were successfully predicted and compared with experiments. An improved two-phase mixture model was later proposed by Wang [18] to cover the simulation in all zones of the porous media as phase change occurs. The new numerical scheme was validated with their experimental results. Zhao and Liao [19] used the new model to study boiling heat transfer in a vertical packed bed. Different flow directions were investigated. Their results showed that the direction of the incoming fluid had great influence on both the flow field and temperature distribution. Najjari and Nasrallah [20,21] conducted several studies on the heat transfer in the conjugated domain with an open layer above the porous layer. The two-phase mixture model was used to treat the fluid flow and heat transfer in the porous layer. The effects of latent heat storage and the thickness of the porous layer on the heat transfer were investigated. Yuki et al. [22] modified the two-phase mixture model to study high flow velocity in the porous media. Their results showed that the modified equations produced more realistic and reasonable results for the two-phase flow under high velocity and high heat flux.

A good heat sink in a cooling system is crucial for effective heat removal. It has been shown that heat sinks made of porous media with high thermal conductivity and large surface area can improve heat transfer performance greatly. A relatively new porous media was developed at Oak Ridge National Laboratory (ORNL), USA [23]. It consists of predominantly spherical pores with small openings between the ligaments. The properties of this material are well documented in the work of Klett et al. [24]. The prominent advantages of this material make it a promising material for many thermal management applications [25,26].

The study of the transient two-phase flow and heat transfer in the porous media is important since it can provide more detailed information on the phase change process. Although many studies have been reported on two-phase flow using the two-phase mixture model, transient fluid flow and heat transfer in the porous media have not been investigated in depth. Currently, there is no detailed information on the treatment of the discontinuity in the diffusion coefficient in the aforementioned works. Therefore, the objective of the present work is to study transient two-phase flow and heat transfer in a discretely heated channel filled with porous media. The two-phase mixture model is adopted to describe momentum and energy transport in the system. Two different numerical schemes, i.e. the harmonic mean method and the "modified" Kirchhoff method [27], were adopted to cope with the sharp discontinuity in the diffusion coefficient. Three cases with discrete heat flux applied from different locations *viz.* (1) lower wall, (2) upper wall and (3) both the lower and upper walls were considered. The vapor generated for each of these cases was analyzed.

2. Mathematical formulation

2.1. Problem description

The present work studies the two-phase flow and heat transfer in a channel fully filled with a porous medium. The schematic of the problem is shown in Fig. 1. A discrete heat flux, at the lower wall [Fig. 1(a)], the upper wall [Fig. 1(b)], and both the lower and upper walls [Fig. 1(c)], is imposed in turn on the domain. These are henceforth referred to as bottom heated (BH), top heated (TH), and bottom and top heated (BTH) cases, respectively. The non-heated portion of the wall is adiabatic. As the sub-cooled water with low temperature T_{in} flows into the channel, convection heat transfer occurs between the heated wall and the fluid. When the heat flux is increased, boiling occurs at the heated surface and thus a two-phase zone is formed. Further increase in the heat flux will lead to a superheated vapor zone. This could cause dry-out in which no liquid exists on the heated surface. The vapor layer blankets the heated surface and greatly reduces the heat transfer between the heated surface and the liquid. Consequently, the local temperature

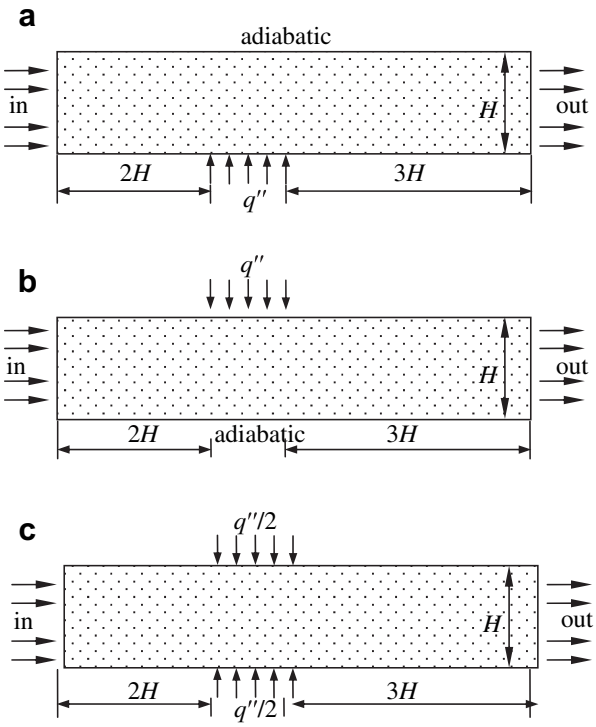

Fig. 1. Schematic of the problem (a) BH; (b) TH; (c) BTH.

at the dry-out location increases sharply. This is unfavorable to the cooling system. Hence, the present work considers only the case without any occurrence of a superheated vapor zone.

2.2. Governing equations

The present model considers an isotropic and homogeneous porous medium. The local thermal equilibrium model which assumes that the solid and fluid phases are at the same temperature is used here. The governing equations by adopting the two-phase mixture model [18] can be written as:

Conservation of mass:

$$\varepsilon\frac{\partial\rho}{\partial t}+\nabla(\rho\boldsymbol{u}) = 0 \tag{1}$$

Conservation of momentum:

$$\boldsymbol{u} = -\frac{K}{\mu}[\nabla p-(\rho_k-\rho_o)\boldsymbol{g}] \tag{2}$$

Conservation of energy:

$$\Omega\frac{\partial h}{\partial t}+\nabla(\gamma_h\boldsymbol{u}h) = \nabla(\Gamma_h\nabla h)+\nabla\left[f(s)\frac{K\Delta\rho h_{fg}}{\nu_v}\boldsymbol{g}\right] \tag{3}$$

The mixture variables and the properties in Eqs. (1)–(3) are listed in Table 1. The temperature and liquid saturation s can be calculated from the enthalpy as

$$T = \begin{cases} \dfrac{h+2\rho_l h_{vsat}}{\rho_l C_{pl}} & h\le-\rho_l(2h_{vsat}-h_{lsat}) \\ T_{sat} & -\rho_l(2h_{vsat}-h_{lsat}) < h\le-\rho_v h_{vsat} \\ T_{sat}+\dfrac{h+\rho_v h_{vsat}}{\rho_v C_{pv}} & -\rho_v h_{vsat} < h \end{cases} \tag{4}$$

Table 1
Variables in the two-phase mixture model.

Variables	Expressions
Density	$\rho = \rho_l s+\rho_v(1-s)$
Velocity	$\rho\boldsymbol{u} = \rho_l\boldsymbol{u}_l+\rho_v\boldsymbol{u}_v$
Enthalpy	$\rho h = \rho_l s h_l+\rho_v(1-s)h_v$
Kinetic density	$\rho_k = \rho_l[1-\beta_l(T-T_o)]\lambda_l(s)+\rho_v[1-\beta_v(T-T_{sat})]\lambda_v(s)$
Viscosity	$\mu = \dfrac{\rho_l s+\rho_v(1-s)}{k_{rl}/\nu_l+k_{rv}/\nu_v}$
Advection correction coefficient	$\gamma_h = \dfrac{[(\rho_v/\rho_l)(1-s)+s][h_{vsat}(1+\lambda_l)-h_{lsat}\lambda_l]}{(2h_{vsat}-h_{lsat})s+(\rho_v h_{vsat}/\rho_l)(1-s)}$
Effective heat capacitance ratio	$\Omega = \varepsilon+\rho_s C_{ps}(1-\varepsilon)\dfrac{dT}{dH}$
Effective diffusion coefficient	$\Gamma_h = \dfrac{1}{1+(1-\rho_v/\rho_l)h_{vsat}/h_{fg}}D+k_{eff}\dfrac{dT}{dH}$
Capillary diffusion coefficient	$D_s = \dfrac{(\varepsilon K)^{0.5}\sigma}{\mu_l}\dfrac{k_{rl}k_{rv}}{(\nu_v/\nu_l)k_{rl}+k_{rv}}[-J'(s)]$
Relative motilities	$\lambda_l(s) = \dfrac{k_{rl}/\nu_l}{k_{rl}/\nu_l+k_{rv}/\nu_v}$, $\lambda_v(s) = \dfrac{k_{rv}/\nu_v}{k_{rl}/\nu_l+k_{rv}/\nu_v}$
Hindrance function	$f(s) = \dfrac{k_{rv}k_{rl}/\nu_l}{k_{rl}/\nu_l+k_{rv}/\nu_v}$
Relative permeabilities	$k_{rl} = s^3$, $k_{rv} = (1-s)^3$
Capillary pressure function	$J(s) = 1.417(1-s)-2.120(1-s)^2+1.263(1-s)^3$

$$s = \begin{cases} 1 & h\le-\rho_l(2h_{vsat}-h_{lsat}) \\ \dfrac{h+\rho_v h_{vsat}}{\rho_l h_{fg}+(\rho_l-\rho_v)h_{vsat}} & -\rho_l(2h_{vsat}-h_{lsat}) < h\le-\rho_v h_{vsat} \\ 0 & -\rho_v h_{vsat} < h \end{cases} \tag{5}$$

Subscripts l and v in Eqs. (4) and (5) refer to the liquid and vapor, respectively. The individual velocities of the liquid and vapor can be recovered from

$$\rho_l\boldsymbol{u}_l = \lambda_l\rho\boldsymbol{u}+\boldsymbol{j} \tag{6}$$

$$\rho_v\boldsymbol{u}_v = \lambda_v\rho\boldsymbol{u}-\boldsymbol{j} \tag{7}$$

where $\boldsymbol{j}$ is the total mass flux which is expressed as

$$\boldsymbol{j} = -\rho_l D(s)\nabla s+f(s)\frac{K\Delta\rho}{\nu_v}\boldsymbol{g} \tag{8}$$

2.3. Boundary conditions

The initial and boundary conditions for the present problem are given as follows:

At $t = 0$,

$$h = \rho_l(C_{pl}T_{in}-2h_{vsat}) \tag{9}$$

$$u = v = 0 \tag{10}$$

At the inlet $x = 0$ and $t > 0$,

$$h = \rho_l(C_{pl}T_{in}-2h_{vsat}) \tag{11}$$

$$u = 6u_{in}\frac{y(H-y)}{H^2} \tag{12}$$

At the outlet $x = L$ and $t > 0$,

$$\frac{\partial h}{\partial x} = 0 \tag{13}$$

$$\frac{\partial u}{\partial x} = \frac{\partial v}{\partial x} = 0 \tag{14}$$

At the position of the wall that is heated with constant heat flux and $t > 0$,

$$-\frac{\Gamma_h}{\rho}\frac{\partial h}{\partial y} - f(s)\frac{K\Delta\rho h_{fg}}{\nu_v}\boldsymbol{g} = q'' \tag{15}$$

$$u = v = 0 \tag{16}$$

At the position of the wall that is non-heated and $t > 0$,

$$-\frac{\Gamma_h}{\rho}\frac{\partial h}{\partial y} - f(s)\frac{K\Delta\rho h_{fg}}{\nu_v}\boldsymbol{g} = 0 \tag{17}$$

$$u = v = 0 \tag{18}$$

2.4. Numerical procedure

The momentum equation [Eq. (2)] is different from the traditional Navier–Stokes equation. In the present problem, the momentum equation [Eq. (2)] is first substituted into the continuity equation [Eq. (1)] to obtain the equation for pressure. The resulting pressure equation is solved by a line-by-line tri-diagonal matrix algorithm. With the results of the pressure, the mixture velocity field can be calculated using the momentum equation [Eq. (2)]. The individual velocities of the liquid and vapor can be obtained from the mixture velocity using Eqs. (6) and (7). These velocities are stored at the interfaces of the control volumes. The energy equation [Eq. (3)] can be written as a general convective–diffusive equation of the form

$$\frac{\partial(\rho\phi)}{\partial t} + \frac{\partial(\rho u_j\phi)}{\partial x_j} = \frac{\partial}{\partial x_j}\left(\Gamma\frac{\partial\phi}{\partial x_j}\right) + S \tag{19}$$

where ϕ, Γ and S are defined as the dependent variables, diffusion coefficient and source term in the finite-volume method (FVM) literature [28]. These equations were solved using FVM [28]. The power-law was used to treat the combined convection–diffusion term. A relative error of less than 10^{-6} is required for both the velocity and temperature fields between successive iterations to achieve convergence.

2.5. Code validation

The present code was validated against the experimental results of Easterday et al. [29]. Two-phase flow through a channel completely filled with a porous medium was investigated in their work. The lower wall of the channel between 1/3L and 2/3L along the flow direction was subjected to a constant heat flux. Fig. 2(a) and (b) show that there is reasonable agreement between the present simulation and the experimental results of Easterday et al. [29] for $u_{in} = 0.35$ mm/s. However, large discrepancies between the experiments and numerical simulation are observed around the locations with steep temperature gradient. These can be attributed to several causes. Firstly, the use of some constitutive relationships from the literature which include the effective thermal conductivity, the capillary pressure and others, may not correspond exactly to the conditions of the experiments. Secondly, thermal dispersion is not included in the simulation. Thirdly, steep temperature gradients exist in the thermocouple probe locations. Accurate measurement of the temperature is extremely difficult. Finally, the three-dimensional effect may be important in the experimental setup while the current simulation is only two-dimensional.

2.6. Treatment of the diffusion coefficient

In modeling a phase change problem, treatment of the discontinuous diffusion coefficient at the phase change boundary presents an important challenge. The variation of diffusion coefficient with liquid saturation s in the current problem is shown in Fig. 3(a). The diffusion coefficient is a strong function of s which in turn is highly dependent on temperature, as well as enthalpy. As seen from Fig. 3(a), the diffusion coefficient encounters a sharp and discontinuous variation, *viz.* from around 10^{-6} at $s = 1$–0 for a slight change in s. The same phenomenon occurs as s changes from non-zero to 0. This type of problem requires careful consideration.

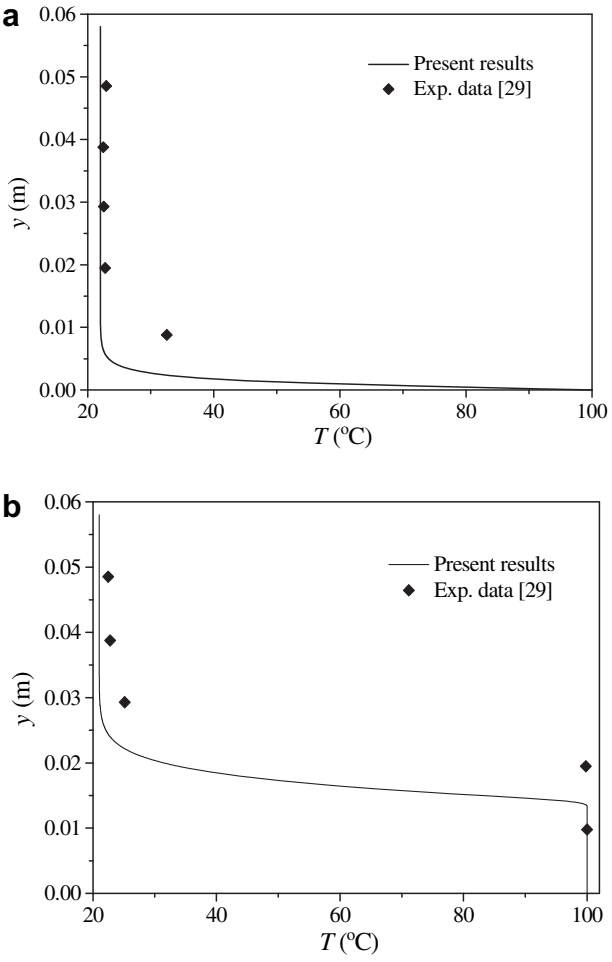

Fig. 2. Comparison of the simulation and the experimental results of Easterday et al. [29] for (a) $x = 1/3L$; (b) $x = 1/2L$.

Several numerical schemes have been proposed to deal with the discontinuity in the diffusion coefficient [27,28,30]. One popular scheme is the harmonic mean method. A detailed description of this method can be found in the work of Patankar [28]. Voller and Swaminathan [27] developed a new scheme based on the local Kirchhoff transformation [31] which is mathematically expressed as

$$\phi = \int_{T_{ref}}^{T} \Gamma(\alpha)d\alpha \tag{20}$$

After some mathematical manipulations, the equivalent expressions of $\Gamma(\alpha)$ are [27]

$$\Gamma_x(\alpha) = \frac{\partial\phi}{\partial x} \quad \Gamma_y(\alpha) = \frac{\partial\phi}{\partial y} \tag{21}$$

With reference to Eqs. (20) and (21), the central difference approximations of the interface diffusion coefficient can be written as

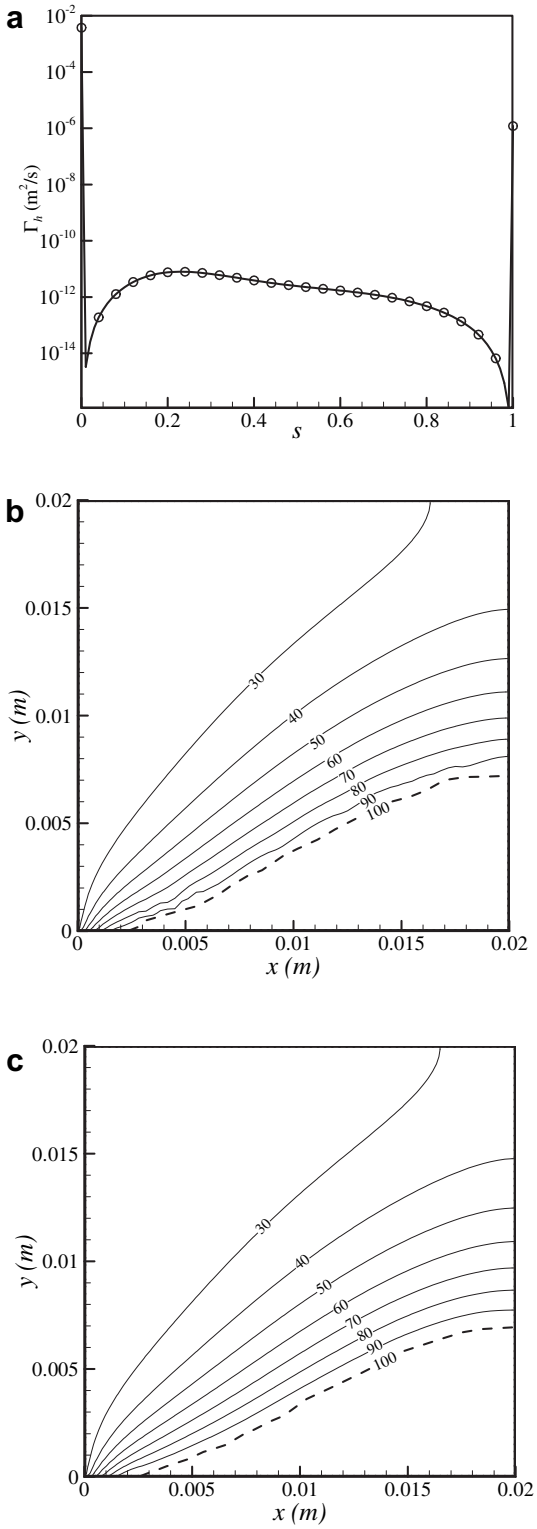

Fig. 3. (a) Diffusion coefficient against s and temperature contours obtained using the (b) harmonic mean method, and (c) "modified" Kirchhoff method.

$$\Gamma_e = \frac{\phi_E - \phi_P}{T_E - T_P} \quad \Gamma_w = \frac{\phi_P - \phi_W}{T_P - T_W} \tag{22}$$

$$\Gamma_n = \frac{\phi_N - \phi_P}{T_N - T_P} \quad \Gamma_s = \frac{\phi_P - \phi_S}{T_P - T_S} \tag{23}$$

Eqs. (22) and (23) are the new scheme proposed by Voller and Swaminathan [27] who termed it the "modified" Kirchhoff method. The current work will adopt the same terminology for easy reference. However, unlike the work of Voller and Swaminathan [27] where the integral variable is temperature, the present article adopts enthalpy h, as the integral variable given the form of the energy equation expressed in terms of enthalpy. The performance of the harmonic mean method and the "modified" Kirchhoff method in resolving the discontinuous diffusion coefficient will be compared. A square channel completely filled with a porous medium is used to test these two methods. Fluid flows through the channel with constant heat flux at the lower wall. The length and the width of the channel are both 20 mm. The properties of the porous medium in the current study were measured and reported in a previous experimental study by the authors [32]. The porosity of the porous medium is 0.75 with absolute permeability of 7.74×10^{-10} m^2. The effective thermal conductivity for water flow through the porous media is calculated based on the model proposed by Tee et al. [33]. A parabolic velocity profile with an average velocity of 1 mm/s is imposed at the inlet. The heat flux is set to 400 kW/m^2. A time-step size of $\Delta t = 0.5$ s with 60×60 control volumes is found to produce grid-independent results. The steady-state temperature distributions from the harmonic mean and "modified" Kirchhoff methods are shown in Fig. 3(b) and (c), respectively. The dashed lines in both figures indicate the interface of the sub-cooled liquid zone and two-phase zone. As seen from Fig. 3(b), both the 80 °C and 90 °C isotherms are not smooth. Although the use of the "modified" Kirchhoff method involves an integral of Eq. (20) which requires additional calculations, all the temperature contours are rather smooth. Meanwhile, in the process of the numerical iteration, more rapid convergence is attained by using the "modified" Kirchhoff method. Hence, in the present simulation, the "modified" Kirchhoff method will be employed.

3. Results and discussion

As mentioned previously, the present study focuses on the transient behavior of two-phase fluid flow and heat transfer in porous media. The effects of discrete heat flux from different locations on the transient flow and temperature fields will be investigated. The height of the channel is H and the length is L. The distances before the fluid flows into and out of the heated section are l_1 and l_2, respectively. The channel is completely filled with porous media. For all cases studied, the height of the channel is 20 mm. l_1/H and l_2/H are set to 2 and 3, respectively to ensure that the inlet and exit boundary conditions have no effect on the solution. Water enters the domain with a parabolic velocity profile. The average velocity at the inlet is 0.2 mm/s and the inlet temperature is 22 °C. For both BH and TH cases, a heat flux $q'' = 100$ kW/m^2 was imposed at the wall between the positions of l_1 and l_2 along the flow direction. For the BTH case, the heat fluxes at the bottom and the top heated sections were set to 50 kW/m^2 resulting in a total heat flux of 100 kW/m^2. These heat fluxes were applied at the same axial location as the aforementioned two cases on the upper and lower walls.

A grid independence study was carried out and the results show that a mesh of 360×60 control volumes with $\Delta t = 0.5$ s produces a grid-independent solution. All subsequent computations were performed using this time-step and mesh size.

3.1. Discrete heat flux at the lower wall – the BH case

Figs. 4–6 show the transient behavior of the fluid flow and heat transfer for the case where the lower wall is discretely heated. In the figures, the interface between the sub-cooled liquid zone and

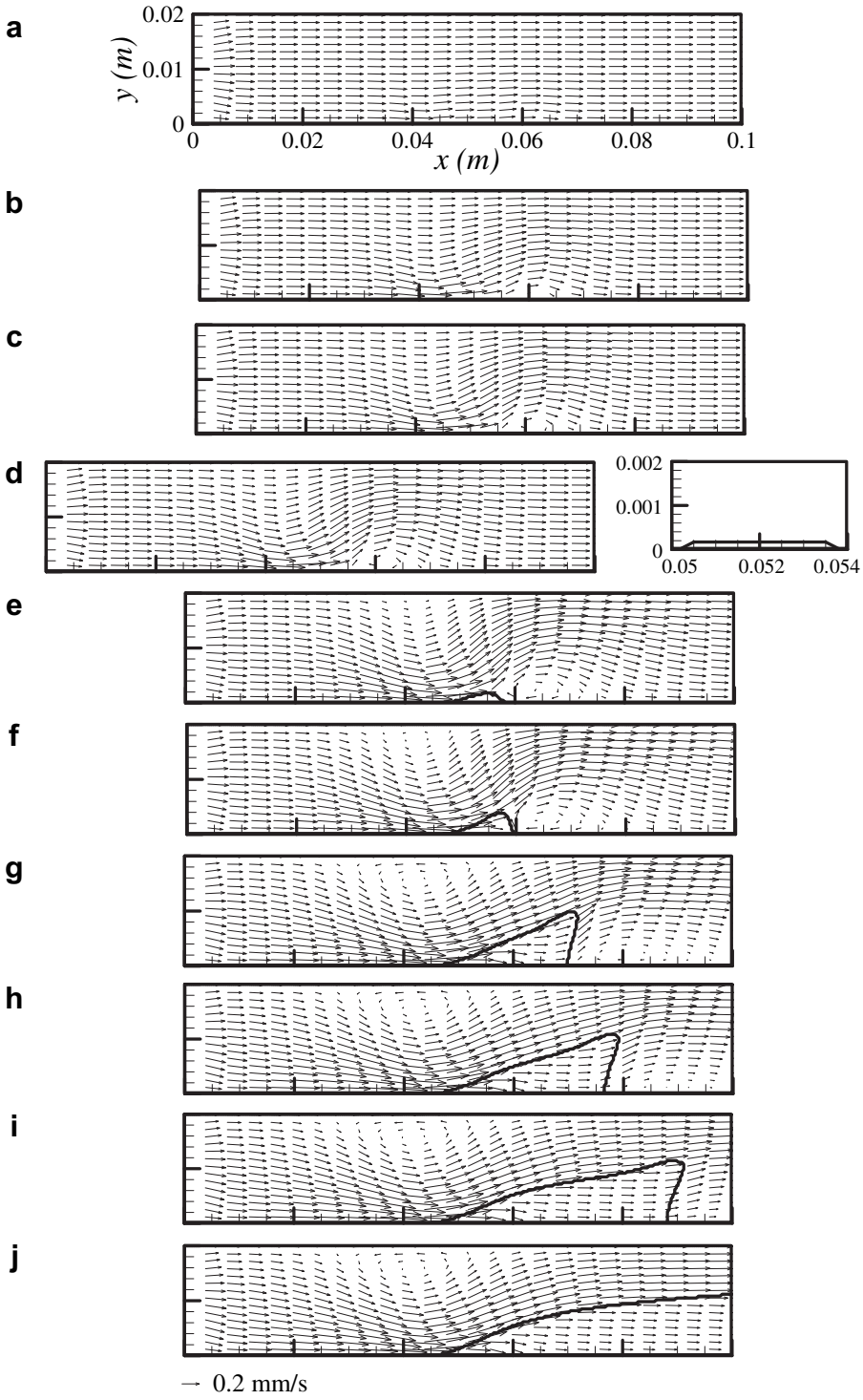

Fig. 4. Liquid velocity vectors at (a) 2 s; (b) 10 s; (c) 15 s (d) 18 s; (e) 40 s; (f) 60 s; (g) 150 s; (h) 190 s; (i) 250 s; (j) 1000 s.

the two-phase zone, also known as the condensation front, is shown as a bold solid line. The temperature in the two-phase zone remains at 100 °C. The liquid saturation inside the sub-cooled zone is 1. In Fig. 6, the numbers on the isotherms in the sub-cooled liquid zone are the temperatures. The numbers inside the two-phase zone are the values of the liquid saturation s. At $t = 0$, liquid flows into the channel with a parabolic velocity profile. At the same time, the discrete heat flux at the lower wall is activated. Within a short distance from the inlet, the flow becomes uniform [Fig. 4(a)]. This is characteristic of a porous medium. Heat is conducted from the heated surface to the solid portion of the porous medium, and then transferred to the liquid flowing through the empty space near the heated surface. The temperature of the liquid near the heated surface increases [Fig. 6(a)] and its density decreases. Acted upon by the buoyancy force, the liquid deflects upward slightly after flowing past the heated surface. At this moment of time, since the density variation is small due to the small temperature difference, the buoyancy force remains small and its effect is less obvious.

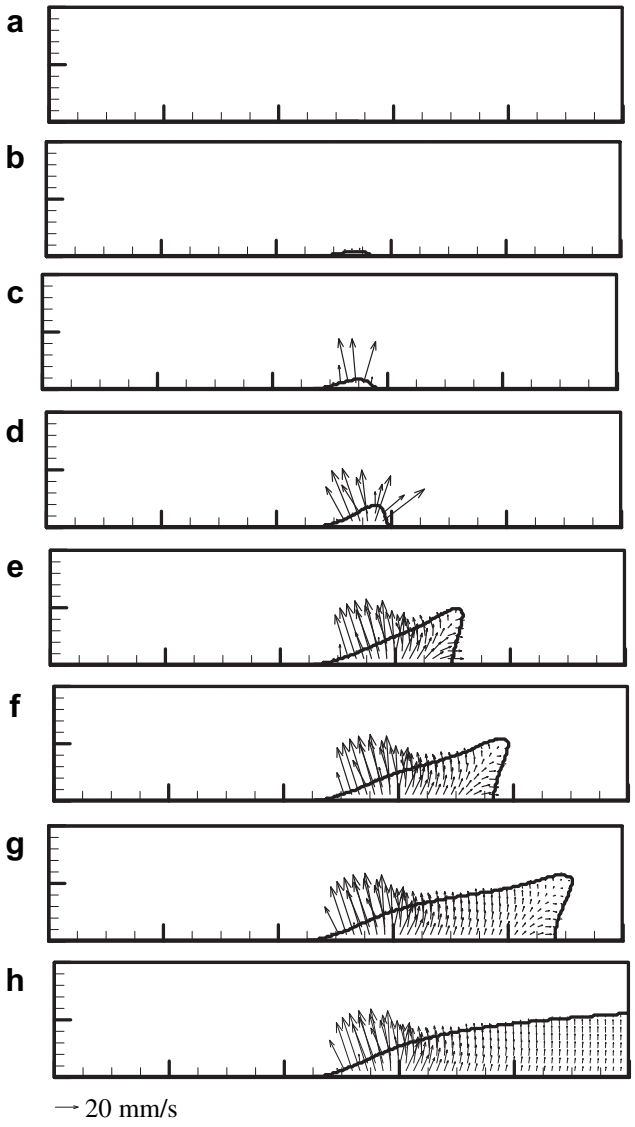

Fig. 5. Vapor velocity vectors at (a) 18 s; (b) 25 s; (c) 40 s; (d) 60 s; (e) 150 s; (f) 190 s; (g) 250 s; (h) 1000 s.

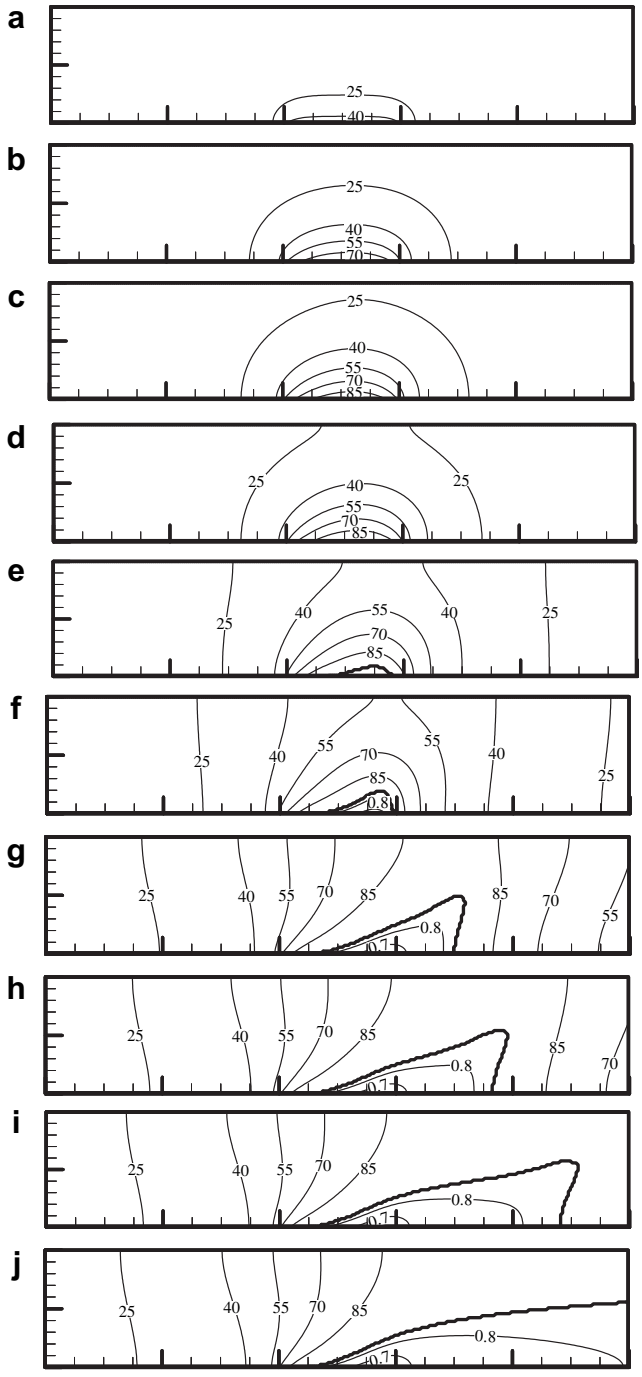

Fig. 6. Temperature and liquid saturation contours at (a) 2 s; (b) 10 s (c) 15 s; (d) 18 s; (e) 40 s; (f) 60 s; (g) 150 s; (h) 190 s; (i) 250 s; (j) 1000 s.

This will however change upon further heating. At $t = 10$ s, as seen from Fig. 4(b) and given the large temperature difference [Fig. 6(b)], the buoyancy force on the liquid becomes stronger and its effect on the flow field is now obvious. The liquid upstream of the heated surface flows downward and towards the heated surface given its lower temperature and higher density. Upon leaving the heated surface, it flows downstream upwardly after being heated. With continued heating, at $t = 15$ s, the effect of the buoyancy on the liquid becomes so significant that it changes the flow structure. The upwardly direct flow of the liquid near the heated surface and the downwardly direct flow of the liquid away from the heated surface create a circulatory flow at the rear of the heated surface [Fig. 4(c)]. Prior to this, the temperature contours have approximately the "dome" shape covering the heated surface [Fig. 6(a) and (b)]. These profiles are similar to the two-dimensional conduction profiles until the flow structures change. The circulatory flow which occurred at $t = 15$ s changes the shapes of the temperature contours slightly [Fig. 6(c)]. The isotherms are seen to be slightly sparser at the back of the heated surface compared to those at the leading edge of the heated surface, indicating poorer heat transfer. The heat absorbed by the circulatory flow is mainly transferred to the main stream by conduction rather than by convection. This is not favorable to heat transfer.

The onset of phase change occurs around $t = 18$ s as seen from Fig. 4(d). A two-phase zone, although extremely thin, forms just above the heated surface. This can be seen in the view of the enlarged figure at the relevant location adjacent to the heated surface. The two-phase zone contains both liquid and vapor coexisting together. Only a small amount of liquid becomes vapor at this time. The generated vapor inside the two-phase zone covers the heated surface and heat transfer from the heated surface to the fluid is thus reduced. The quantity of vapor at this time is sufficiently

small so that its effect on the velocity field is not obvious [Fig. 5(a)]. At $t = 40$ s, the two-phase zone expands [Fig. 4(e)] as more liquid vaporizes. The density of the vapor is much lower than the liquid. Therefore, the generated vapor flows upwards [Fig. 5(c)] due to the buoyancy force which, simultaneously, leads to the expansion of the two-phase zone. As heating continues, the density difference between the liquid from the incoming upstream and the liquid adjacent to the condensation front is further increased. Most of the incoming liquid in the sub-cooled liquid zone, referred to as the main stream from henceforth, flows downwardly to the heated surface. As it approaches the condensation front, the main stream turns upward because it is heated and becomes lighter. The formed vapor in the two-phase zone occupies the pores partially reducing the permeability for liquid flow through the two-phase zone. This also helps to deflect the liquid upward. After flowing through the two-phase zone, the accelerated main stream flows downward and exerts a larger shear force on the liquid at the rear of the two-phase zone, thus, increasing the strength of the vortex. With the occurrence of the two-phase zone, the dome-shaped temperature contours changes totally. The isotherms in the leading edge of the heated surface are inclined in an upward fashion towards the outlet [Fig. 6(e)] due to the incoming sub-cooled liquid.

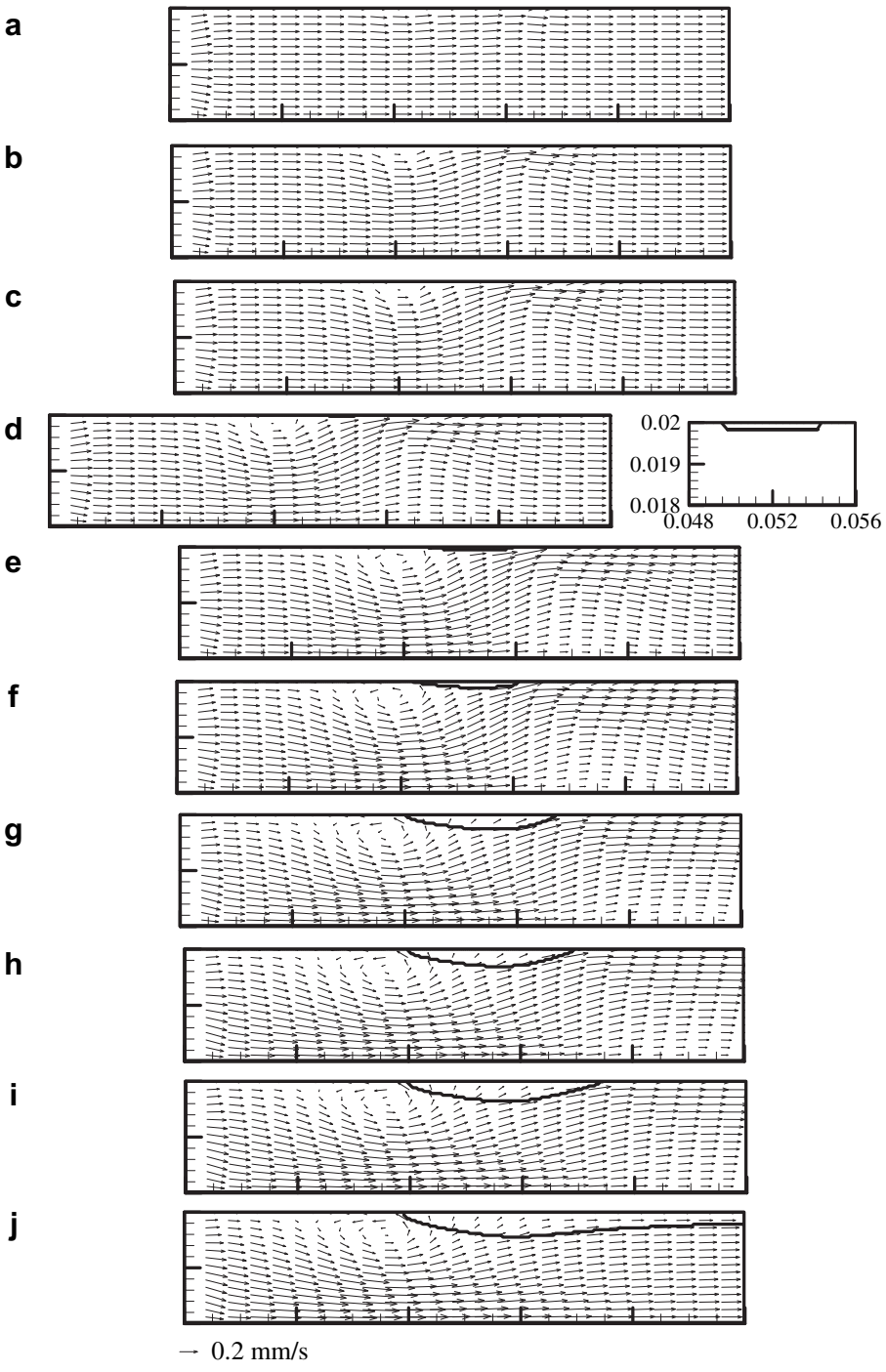

Fig. 7. Liquid velocity vectors at (a) 2 s; (b) 10 s; (c) 15 s; (d) 21 s; (e) 40 s; (f) 60 s; (g) 150 s; (h) 190 s; (i) 250 s; (j) 1000 s.

At $t = 60$ s, the downward flow of the incoming main stream becomes so significant that only a small portion of liquid flows near the upper wall. The liquid with low velocity adjacent to the upper wall is counteracted by the deflected main stream passing the two-phase zone, resulting in another circulatory flow [Fig. 4(f)]. The vapor, driven by both capillary-induced and buoyancy-induced forces, flows partially upwards to the inlet and outlet [Fig. 5(d)]. The newly emerged vortex adjacent to the upper wall forces the incoming liquid to flow downwards, and thus reduces the heat transfer in the locations near the vortex. This is reflected by the changes to the isotherms of $T = 25$ °C and $T = 40$ °C from Fig. 6(e) and (f). The minimum liquid saturation s is found to be at the location above the heated surface. With the expansion of the two-phase zone, the vortex at the rear of the two-phase zone is pushed further downstream [Fig. 4(f)]. As heat is being transferred, the temperature difference of the main flow leaving the two-phase zone is reduced [Fig. 6(g)] thus reducing its density difference. This gradually suppressed the vortex at the rear of the two-phase zone [Fig. 4(g)]. The vapor inside the two-phase zone splits into three streams at this time [Fig. 5(e)], with one towards the upstream at the front, the other flowing downstream at the back, and the left stream flowing upwards to the upper wall in the middle. At $t = 190$ s, the vortex at the rear of the two-phase zone is totally suppressed. Affected slightly by the buoyancy force, the liquid at the rear of the two-phase zone flows upward. This stream of liquid becomes parallel as the two-phase zone expands to the outlet as shown in Fig. 4(j) for $t = 1000$ s. At this time, steady state has been achieved. The majority of the vapor above the non-heated surface

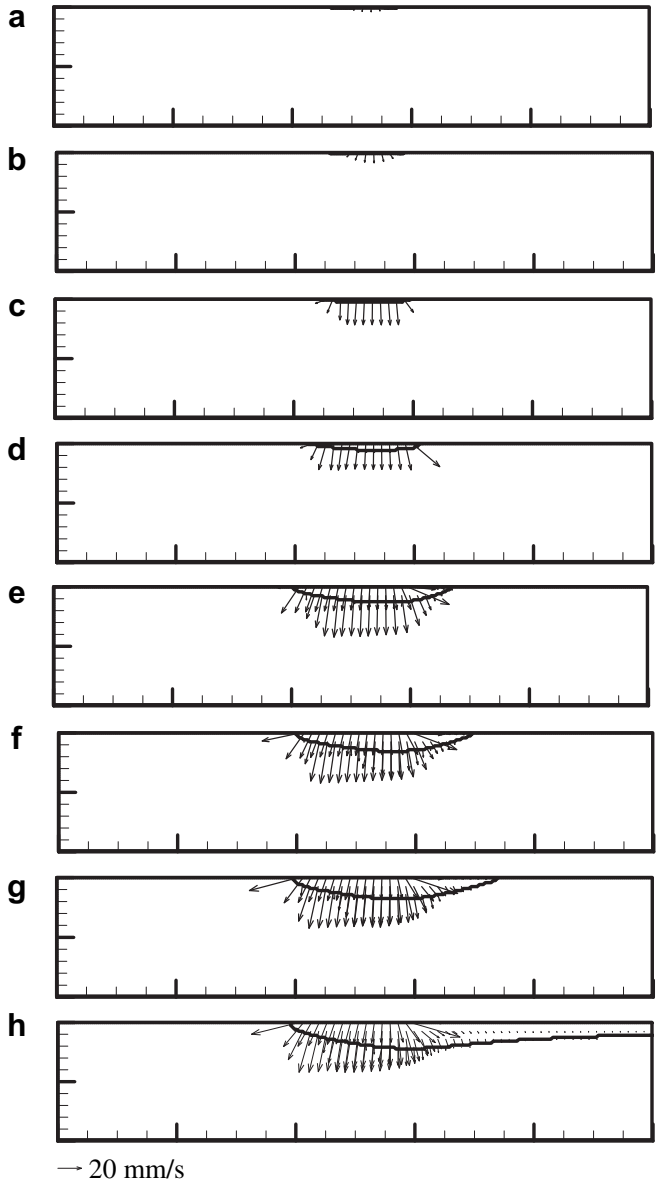

Fig. 8. Vapor velocity vectors at (a) 28 s; (b) 30 s; (c) 40 s; (d) 60 s; (e) 150 s; (f) 190 s; (g) 250 s; (h) 1000 s.

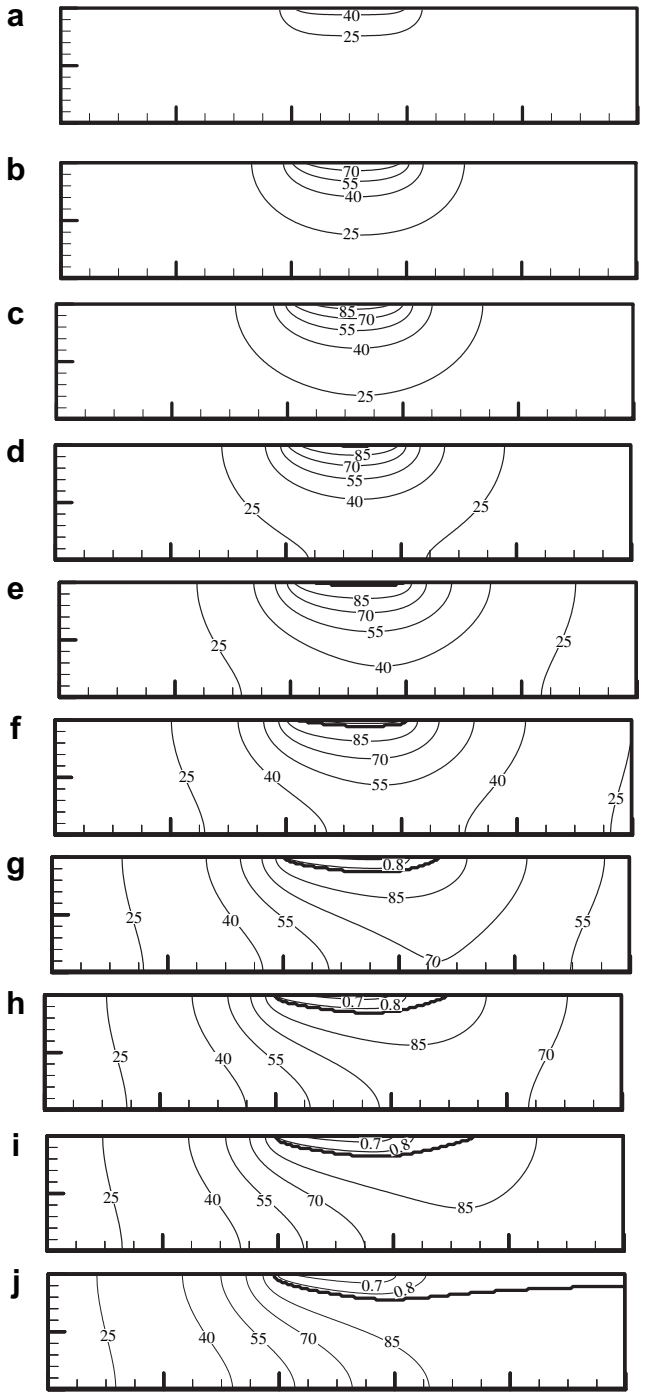

Fig. 9. Temperature and liquid saturation contours at (a) 2 s; (b) 10 s; (c) 15 s; (d) 21 s; (e) 40 s; (f) 60 s; (g) 150 s; (h) 190 s; (i) 250 s; (j) 1000 s.

flows directly upwards because of the buoyancy force [Fig. 5(h)]. Note that vapor from the heated surface flows to the condensation front in a normal direction.

3.2. Discrete heat flux at the upper wall – the TH case

The case with discrete heat flux imposed from the upper wall at the same axial location as the BH case is now discussed. Figs. 7–9 show the evolutions of the fluid velocity and temperature profiles. At the beginning of the heating, the liquid has a similar flow profile [Fig. 7(a)] as in the BH case. The temperature contours show the reversed "dome" shape [Fig. 9(a)]. However, this will change upon further heating. Driven by the buoyancy force, the liquid with high temperature and low density below the heated surface of the upper wall flows upward. The upstream parallel flow from the inlet is counteracted by this buoyancy-induced upward flow of the liquid, resulting in a circulatory flow in the leading edge of the heated surface [Fig. 7(c)].

The onset of boiling occurs at $t = 21$ s [Fig. 7(d)], 3 s later than that in the BH case. The buoyancy force drives the high temperature liquid to flow towards the heated surface of the upper wall, diminishing the convection heat transfer between the heated

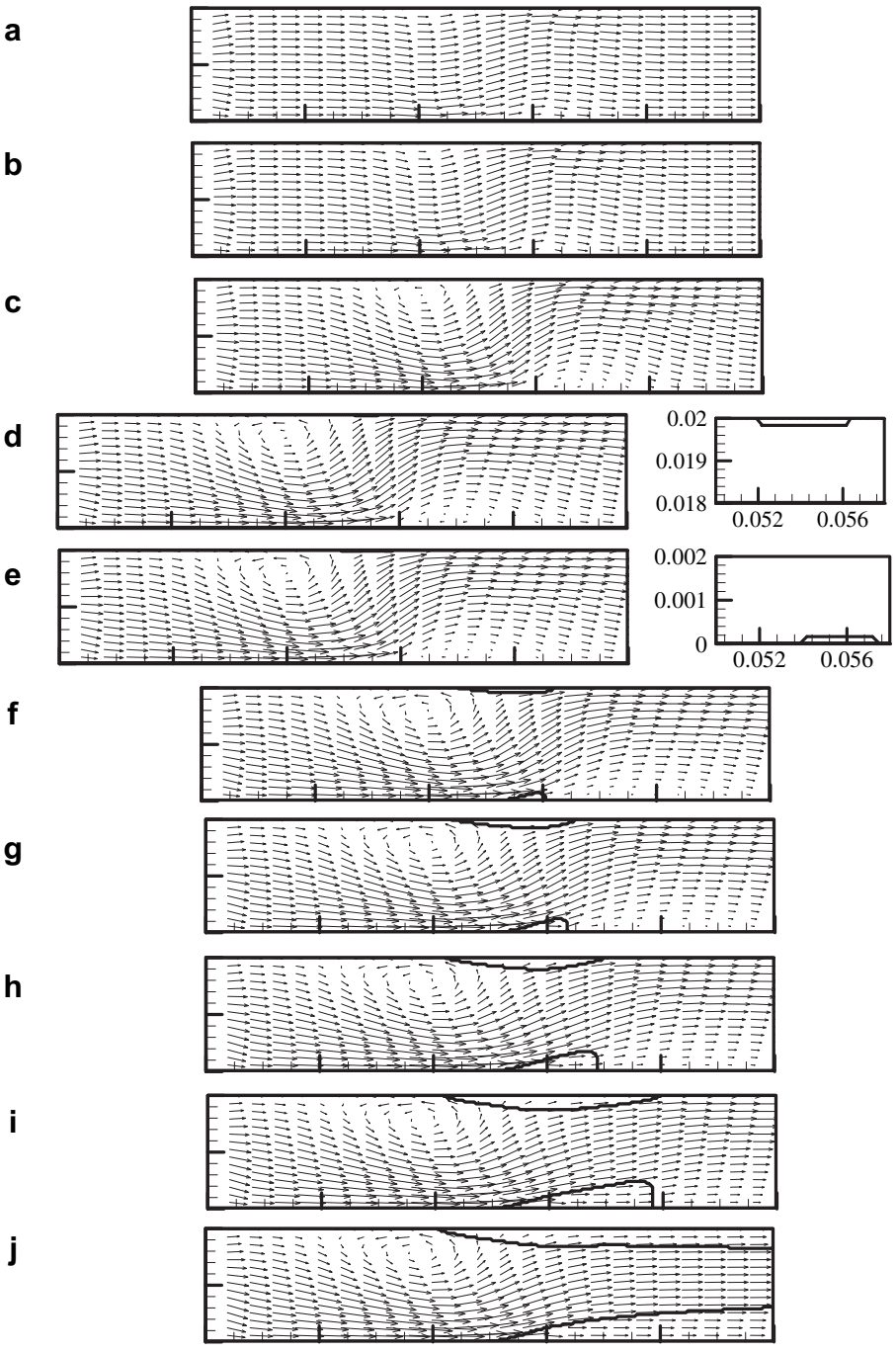

Fig. 10. Liquid velocity vectors at (a) 10 s; (b) 15 s; (c) 50 s; (d) 75 s; (e) 85 s; (f) 120 s; (g) 150 s; (h) 190 s; (i) 250 s; (j) 1000 s.

surface and the liquid below, which in turn delays the time for the liquid to be heated to its boiling point. At the early stages of phase change, the generated vapor with lower density accumulates on the top of the heated surface due to the buoyancy force. The quantity of the vapor at this stage is extremely small so that its velocity cannot be seen until $t = 28$ s [Fig. 8(a)]. As time progresses, more liquid vaporizes. Since the vapor density is much smaller than the liquid, the volume of the vapor expands, leading to the expansion of the two-phase zone. The velocity vectors of the vapor can be clearly seen in Fig. 8(b). Given the strong incoming sub-cooled liquid flow, the temperature contours with reversed "dome" shape incline slightly to the outlet [Fig. 9(e)]. As heating continues, the two-phase zone expands downward and migrate downstream [Fig. 7(f)]. The main stream, coming from the inlet boundary flows downward to bypass the vortex. Upon reaching the heated surface, it is driven to flow upward towards the condensation front due to the buoyancy force. This is different from the BH case in which the liquid was deflected to bypass the condensation front. Driven by the capillary pressure gradient, it is interesting to note that the liquid in the two-phase zone flows towards the heated surface [Fig. 7(g)], while the vapor in the two-phase zone flows primarily downwards [Fig. 8(e)]. Such counter-percolation movement of the liquid and vapor is the main heat transfer mechanism within the two-phase zone.

As more liquid is vaporized, the two-phase zone assumes the shape of a half-ellipse [Figs. 7(h), 8(f) and 9(h)]. The resulting shape is not only affected by gravity, but also by the upward flow of the liquid as it approaches the condensation front. Under steady state conditions, the upper wall, from the leading edge of the heated surface to the outlet is covered by the two-phase zone, as seen from Figs. 7(j), 8(h) and 9(j) at $t = 1000$ s. The two-phase zone is smaller compared to its counterpart in the BH case.

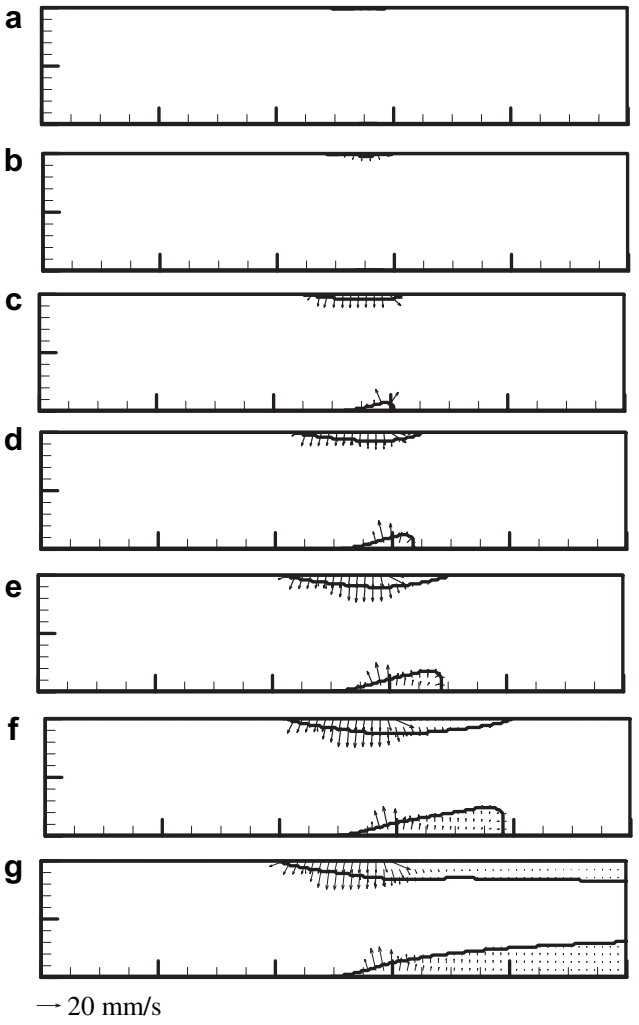

Fig. 11. Vapor velocity vectors at (a) 85 s; (b) 90 s; (c) 120 s; (d) 150 s; (e) 190 s; (f) 250 s; (g) 1000 s.

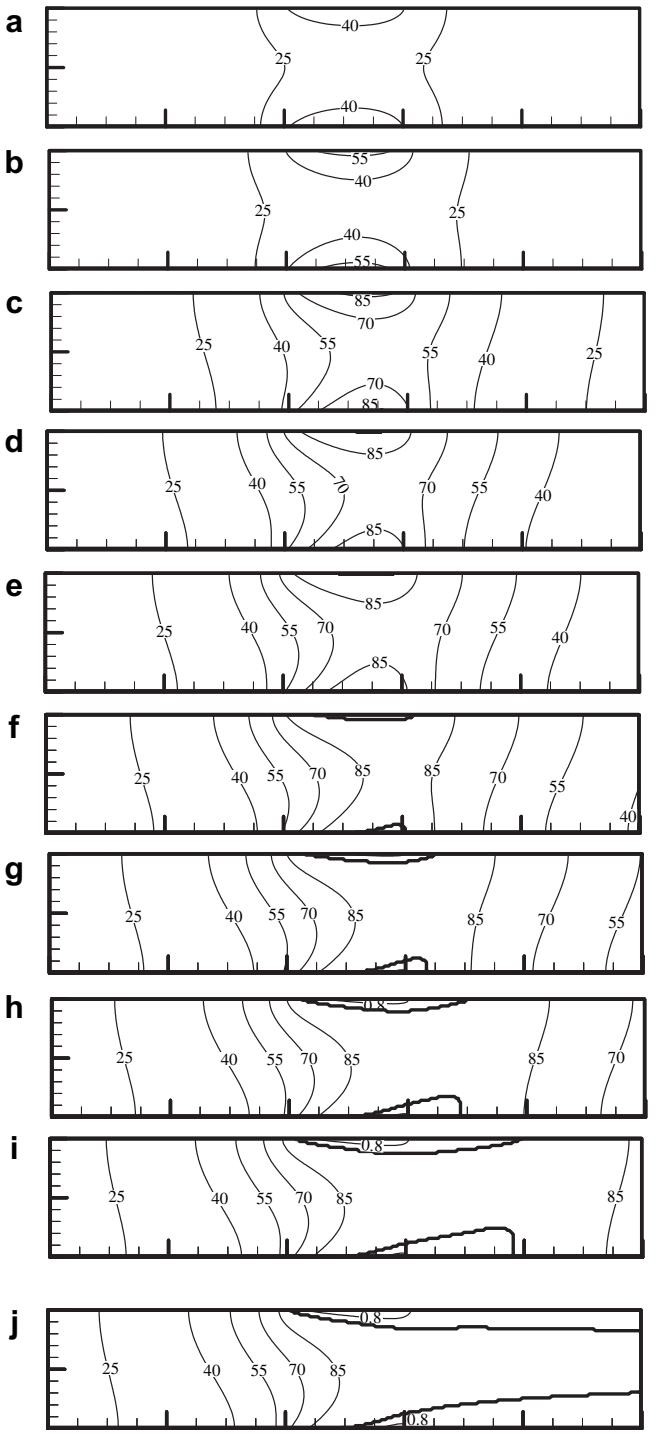

Fig. 12. Temperature and liquid saturation contours at (a) 10 s; (b) 15 s; (c) 50 s; (d) 75 s; (e) 85 s; (f) 120 s; (g) 150 s; (h) 190 s; (i) 250 s; (j) 1000 s.

3.3. Discrete heat flux at both the lower and upper walls – the BTH case

In this third case study, both the upper and lower walls are discretely heated. As the liquid flows across these walls, it absorbs heat from the solid portion of the porous medium. Its temperature increases [Fig. 12(a) and (b)], leading to a smaller density. The liquid motion is now affected by the buoyancy force [Fig. 10(a) and (b)]. The liquid across the heated surface of the lower wall, flows downstream in a slightly upward manner. The liquid upstream of the heated surface of the lower wall, which is cooler and therefore denser, tends to flow downward towards the heated surface of the lower wall to replenish the higher temperature liquid leaving the region above the heated surface of the lower wall. This combination of incoming and outgoing flows to the region above the heated surface of the lower wall is favorable for heat removal from the heated surface of the lower wall. Buoyancy assists to draw cooler fluid towards the heated surface and expel hotter liquid from the region above the heated wall. Heat is convected away to the downstream fluid from the heated surface of the lower wall. This is not the case for the liquid flowing across the heated surface of the upper wall. Buoyancy actually drives the higher temperature liquid upward towards the heated surface of the upper wall. In such a situation, the convection heat transfer between the heated surface of the upper wall and the liquid is reduced. This is not favorable for heat transfer.

The action of the buoyancy force eventually creates two circulatory flows in the channel as shown in Fig. 10(c). These circulatory flows are located upstream of the heated surface of the upper wall and downstream of the heated portion of the lower wall. The circulatory flow near the upper wall is much stronger. The temperature distribution at $t = 50$ s [Fig. 12(d)] is obviously not symmetrical about the middle horizontal plane of the channel. The poorer heat transfer performance for the upper wall results in a generally higher liquid temperature in its adjacent. As time progresses, the liquid adjacent to the heated surface of the upper wall reaches its boiling point earlier than that adjacent to the heated surface of the lower wall. Phase change occurs at around $t = 75$ s at the upper wall [Figs. 10(d) and 12(d)] and later at the lower wall. An extremely thin layer of the two-phase zone covers the heated surface of the upper wall at this time. The vapor velocity at the upper wall is not obvious until $t = 90$ s [Fig. 11(b)] where at this time, the vapor velocity at the lower wall cannot even be clearly noticed.

The two-phase zones at both the upper and lower walls expand as heating continues. The two-phase zone at the lower wall is swept downstream to cover the heated surface of the wall partially [Fig. 11(c)]. On the contrary, the two-phase zone blankets the heated surface of the upper wall entirely [Fig. 11(c)]. The presence of the circulatory flow upstream of the heated surface of the upper actually hinders cooler liquid from reaching the two-phase zone. This results in poorer heat transfer. Driven by the buoyancy force, the vapor on the upper wall attaches to the heated surface. Therefore, the two-phase zone remains thin and is less affected by the liquid flow in the sub-cooled zone at the upper wall. The vapor in the two-phase zone at both the lower and upper walls flows primarily to the condensation front.

With continued heating, the expanded two-phase zone pushes the vortex at the lower wall further downstream [Fig. 10(g)]. The spreading of the heat reduces the temperature difference of the liquid at the downstream of the heated surface [Fig. 12(g)]. This suppresses the buoyancy-induced circulatory flow at the rear of the two-phase zone on the lower wall. At $t = 190$ s, this circulatory flow vanishes [Fig. 10(h)] leaving only the circulatory flow at the upstream of the heated surface on the upper wall. The minimum liquid saturation of 0.8 occurred at the upper wall prior to the lower wall [Fig. 12(h)]. An implication of this result could be that in thermal systems with heat sources at both the lower and upper walls, a dry-out zone could appear at the upper wall. In the steady state [Figs. 10(j), 11(g) and 12(j)], the upper wall, from the leading edge of the heated surface to the outlet, is covered by the two-phase zone, while in the lower wall, the two-phase zone starts from the latter part of the heated surface, showing better heat transfer on the lower wall compared with the upper wall.

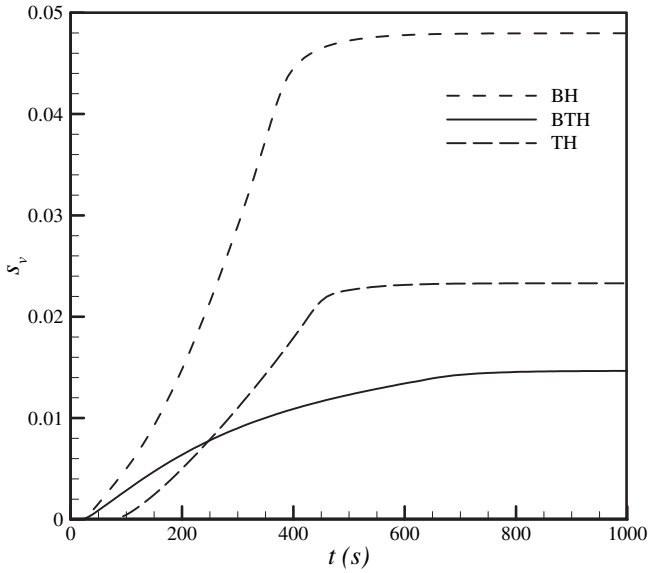

Fig. 13. Time variation of vapor fraction for different cases.

3.4. Variation of the vapor volume fraction

The liquid saturation s is defined as [34]

$$s = \frac{\varepsilon_l}{\varepsilon} \tag{24}$$

where ε is the porosity of the porous media and ε_l is the fraction of the volume occupied by the liquid. According to the above definition, the volume fraction occupied by the generated vapor can be calculated as

$$s_v = \frac{\int_{V_f} 1 dV_f - \int_{V_f} s dV_f}{V_f} \tag{25}$$

where V_f is fluid volume in the porous media. Based on Eq. (25), the variations of s_v with time for different cases are shown in Fig. 13. The BH and BTH cases achieved steady state in a shorter time compared with the TH case, indicating enhanced cooling of the heated surface. The rate of vapor generation, implied by the slope of the lines, in the BH case is the highest among the three cases. The largest volume fraction of vapor is also found in the BH case. This can be attributed to better heat transfer for the case where heating is from the lower wall. The TH case produces a faster generation of the vapor before $t = 250$ s compared with the BTH case. The rate of vapor generation decreases after that, resulting in the smallest amount of the vapor among the three studied cases.

4. Conclusions

A numerical study of the two-phase flow and heat transfer in the channel with porous media was conducted. The harmonic mean

method and the "modified" Kirchhoff method were adopted to treat the discontinuity in the diffusion coefficient. The latter was shown to be better in dealing with the sharp change of the diffusion coefficient. The effects of heating from different locations on the transient behavior of the flow and temperature fields were discussed. The results showed that the location of the heat flux has a significant effect on fluid flow and heat transfer in a channel filled with a porous medium. Both the amount and the generation rate of the vapor in the BH case are the largest among the three cases studied.

Acknowledgment

The authors gratefully acknowledge the financial support provided under Defence Science and Technology Agency, Singapore Grant no. DSTA-NTU-DIRP/2005/01 for the work described in this paper.

References

[1] T. Boberg, Thermal Methods of Oil Recovery. John Wiley, New York, 1988.
[2] A. Faghri, Heat Pipe Science and Technology. Taylor & Francis, Washington, DC, 1995.
[3] O. Chapuis, M. Prat, M. Quintard, E. Chane-Kane, O. Guillot, N. Mayer, Two-phase flow and evaporation in model fibrous media: application to the gas diffusion layer of PEM fuel cells. J. Power Sources 178 (2008) 258–268.
[4] A.A. Mohamad, Heat transfer enhancements in heat exchangers fitted with porous media, part I: constant wall temperature. Int. J. Therm. Sci. 42 (2003) 385–395.
[5] J. Thevenin, D. Sadaoui, About enhancement of heat transfer over a circular cylinder embedded in a porous medium. Int. Commun. Heat Mass Transf. 27 (1995) 295–304.
[6] L.P. Cheng, A.V. Kuznetsov, Heat transfer in a laminar flow in a helical pipe filled with a fluid saturated porous medium. Int. J. Therm. Sci. 44 (2005) 787–798.
[7] V. Bubnovich, M. Toledo, Analytical modeling of filtration combustion in inert porous media. Appl. Therm. Eng. 27 (2007) 1144–1149.
[8] C.H. Sondergeld, D.L. Turcotte, Flow visualization studies of two-phase thermal convection in a porous layer. Pure Appl. Geophys. 117 (1978) 321–330.
[9] H.H. Bau, K.E. Torrance, Boiling in low-permeability porous material. Int. J. Heat Mass Transf. 25 (1982) 45–55.
[10] H.H. Bau, K.E. Torrance, Thermal convection and boiling in a porous medium. Lett. Heat Mass Transf. 9 (1982) 431–441.
[11] H.H. Bau, K.E. Torrance, Low Rayleigh number thermal convection in a vertical cylinder filled with porous materials and heated from below. ASME J. Heat Transf. 104 (1982) 166–172.
[12] C.Y. Wang, C. Beckermann, A two-phase mixture model of liquid–gas flow and heat transfer in capillary porous media, I. Formulation. Int. J. Heat Mass Transf. 36 (1993) 2747–2758.
[13] Z.Q. Chen, P. Cheng, T.S. Zhao, An experimental study of two phase flow and boiling heat transfer in bi-dispersed porous channels. Int. Commun. Heat Mass Transf. 22 (2000) 293–302.
[14] P.S. Ramesh, K.E. Torrance, Stability of boiling in porous media. Int. J. Heat Mass Transf. 33 (1990) 1895–1908.
[15] L.M. Albriola, G.F. Pinder, A multiphase approach to the modelling of porous media contamination by organic compounds I: equation development. Water Resour. Res. 21 (1985) 11–18.
[16] P.S. Ramesh, K.E. Torrance, Numerical algorithm for problems involving boiling and natural convection in porous materials. Numer. Heat Transf., Part B 17 (1990) 1–24.
[17] C.Y. Wang, C. Beckermann, C. Fan, Numerical study of boiling and natural convection in capillary porous media using the two-phase mixture model. Numer. Heat Transf., Part A 26 (1994) 375–398.
[18] C.Y. Wang, A fixed-grid numerical algorithm for two-phase flow and heat transfer in porous media. Numer. Heat Transf., Part B 32 (1997) 85–105.
[19] T.S. Zhao, Q. Liao, Mixed convective boiling heat transfer in a vertical capillary structure heated asymmetrically. J. Thermophys. Heat Transf. 13 (1999) 302–307.
[20] M. Najjari, S.B. Nasrallah, Effects of latent heat storage on heat transfer in a forced flow in a porous layer. Int. J. Therm. Sci. 47 (2007) 825–833.
[21] M. Najjari, S.B. Nasrallah, Heat transfer between a porous layer and a forced flow: influence of layer thickness. Drying Technol. 27 (2009) 336–343.
[22] K. Yuki, J. Abei, H. Hashizume, S. Toda, Numerical investigation of thermofluid flow characteristics with phase change against high heat flux in porous media. ASME J. Heat Transf. 130 (2008) 1–12.
[23] J.W. Klett, Process for making carbon foam, US Patent 6033506 (2000).
[24] J.W. Klett, R. Hardy, E. Romine, High thermal conductivity, mesophase-pitch-derived carbon foam: effect of precursor on structure and properties. Carbon 38 (2000) 953–973.
[25] K.C. Leong, L.W. Jin, Study of highly conductive graphite foams in thermal management applications. Adv. Eng. Mater. 10 (2008) 338–345.
[26] Y.L. Jamin, A.A. Mohamad, Natural convection heat transfer enhancements from a cylinder using porous carbon foam: experimental study. ASME J. Heat Transf. 130 (2008) 122502–122506.
[27] V.R. Voller, C.R. Swaminathan, Treatment of discontinuity thermal conductivity in control-volume solutions of phase change problems. Numer. Heat Transf., Part B 24 (1993) 161–180.
[28] S.V. Patankar, Numerical Heat Transfer and Fluid Flow. Hemisphere Publishing Corporation, 1980.
[29] O.T. Easterday, C.Y. Wang, P. Zheng, A numerical and experimental study of two-phase and heat transfer in a porous formation with localized heating from below. Proc. ASME Heat Transf. Fluid Eng. Divisions 321 (1995) 723–732.
[30] S.L. Lee, R.Y. Tzong, An enthalpy formulation for phase change problems with a large thermal diffusivity jump across the interface. Int. J. Heat Mass Transf. 34 (1991) 1491–1502.
[31] J. Crank, Free and Moving Boundary Problems. Clarendon Press, Oxford, 1984.
[32] L.W. Jin, H.Y. Li, K.C. Leong, J.C. Chai, Heat transfer and air flow through highly conductive graphite foam heat sinks, in: Proc. 7th Int. Symposium on Heat Transfer (IHSR 7), Beijing, China, 2008.
[33] C.C. Tee, J.W. Klett, D.P. Stinton, N. Yu, Thermal conductivity of porous carbon foam, in: Proc. of the 24th Biennial Conference on Carbon, Charleston, USA, 1999.
[34] M. Kaviany, Principles of Heat Transfer in Porous Media, second ed. Springer-Verlag, New York, 1995.